

Mass transfer in eccentric binaries: the new Oil-on-Water SPH technique

R. P. Church^{1,2} \star , J. Dischler¹, M. B. Davies¹, C. A. Tout², T. Adams³ and M. E. Beer³

¹Lund Observatory, Box 43, SE-221 00, Lund, Sweden

²Monash University, Mathematics Department, Clayton, Victoria 3168, Australia

²Institute of Astronomy, The Observatories, University of Cambridge, Madingley Road, Cambridge. CB3 0HA

³Department of Physics and Astronomy, University of Leicester, Leicester. LE1 7RH

Received; Accepted

ABSTRACT

To measure the onset of mass transfer in eccentric binaries we have developed a two-phase SPH technique. Mass transfer is important in the evolution of close binaries, and a key issue is to determine the separation at which mass transfer begins. The circular case is well understood and can be treated through the use of the Roche formalism. To treat the eccentric case we use a newly-developed two phase system. The body of the donor star is made up from high-mass *water* particles, whilst the atmosphere is modelled with low-mass *oil* particles. Both sets of particles take part fully in SPH interactions. To test the technique we model circular mass-transfer binaries containing a $0.6 M_{\odot}$ donor star and a $1 M_{\odot}$ white dwarf; such binaries are thought to form cataclysmic variable (CV) systems. We find that we can reproduce a reasonable CV mass-transfer rate, and that our extended atmosphere gives a separation that is too large by approximately 16%, although its pressure scale height is considerably exaggerated. We use the technique to measure the semi-major axis required for the onset of mass transfer in binaries with a mass ratio of $q = 0.6$ and a range of eccentricities. Comparing to the value obtained by considering the instantaneous Roche lobe at pericentre we find that the radius of the star required for mass transfer to begin decreases systematically with increasing eccentricity.

Key words: gravitation – hydrodynamics – methods: numerical – binaries: close – stars: evolution – stars: mass-loss – X-ray: binaries

1 INTRODUCTION

Mass transfer in binary stars is a very important process that completely changes their evolution. Several eccentric binaries that are undergoing mass transfer exist. One such system is the low-mass X-ray binary Cir X-1 (Murdin et al. 1980; Tauris et al. 1999; Johnston et al. 1999; Clarkson et al. 2004). Its orbital parameters were analysed by Tauris et al. (1999) who argue that the system is probably a $2 M_{\odot}$ star orbiting a neutron star with an eccentricity of about 0.9. Higher mass systems are more frequently observed; one such example is the Be/X-ray transient A0538-66, located in the Large Magellanic Cloud (Kretschmar et al. 2004). This consists of a B2 IIIe star orbiting a neutron star with a period of 16.65 d in an eccentric orbit with $e \approx 0.7$. In most of these systems the mass transfer between the stars is driven by winds rather than through Roche lobe overflow.

Systems such as Cir X-1 are thought to be created when the heavier star explodes in a supernova. Another possible way to create a hard eccentric binary is through a close encounter between a

circular binary and a single star or binary. The rate of such events is only significant when the stellar density is high, so they occur primarily in environments such as the cores of globular clusters (Davies & Benz 1995). For a density of about 10^5 stars/pc³ the average time between close encounters for a system is about 1 Gyr. Hence most of the binaries in a dense globular cluster core undergo at least one encounter.

The theory of mass transfer in the circular case, where the flow is continuous and steady, has been studied for a long time and is well understood (Paczynski 1971; Renvoizé et al. 2002). For two stars in a circular orbit there exists a corotating frame in which they are stationary and if the stars are taken to be point masses the potential, known as the Roche potential, is well defined. The first connected equipotential surface that surrounds both stars is known as the Roche lobe and provides a boundary for the potential well in which the star sits. If we make the assumption that the envelope of the star deforms to the equipotential surface whilst conserving its volume then we can define the Roche lobe radius such that a sphere with that radius has the same volume as the Roche lobe (Eggleton 1983). This can then be used in conjunction with a spherically symmetric model of the stellar structure, such as that produced by a

\star E-mail: ross.church@sci.monash.edu.au

stellar evolution code, to predict the point of onset of mass transfer. The eccentric case is much more difficult because the assumptions made in order to derive the Roche potential are no longer valid. The relative velocities and distances of stars in an elliptic orbit vary so there is no corotating frame.

A commonly used method to assess whether mass transfer occurs in an eccentric binary is to make the assumption that the stars corotate at periastron and apply the circular theory there. However it is not clear that it is possible to define an instantaneous Roche lobe because, among other things, to do so assumes that the timescale upon which the star adjusts to the changing force is sufficiently short (Charles et al. 1983; Brown & Boyle 1984).

Another approach is to simulate such systems numerically. Boyle & Walker (1986) made simulations with test particles placed on the surface of the donor. Haynes et al. (1980) simulated Cir X-1 with a core and an extended atmosphere of test particles. However they only looked at a single orbit. Full numerical simulations of complete systems are rare but Regös et al. (2005) presented some low-resolution smoothed particle hydrodynamic (SPH) simulations where they considered four different eccentricities for a single semi-major axis a and mass ratio q .

In this paper we introduce a new technique (called Oil-on-Water) within the SPH formalism. We define two types of SPH particles, heavy *water* particles that make up the stellar interior and very light *oil* particles that sit on top of the star. We are thus able to resolve the mass transfer even though the fraction of the stellar mass transferred per orbit is very small. We apply this technique to mass transfer in eccentric binaries and investigate a variety of binary systems, varying the semi-major axis a and eccentricity e .

In Section 2 we discuss eccentric mass-transferring binaries from a theoretical point of view, as well as the observational evidence for their existence. In Section 3 the oil-on-water method is described and some tests presented. The results of the simulations are given in Section 4 and discussed in Section 5.

2 THE OIL-ON-WATER TECHNIQUE

In order to investigate mass transfer in eccentric binaries a two-phase SPH technique has been developed. This section describes the new approach and some tests of it.

2.1 Smoothed particle hydrodynamics

SPH was developed by Lucy (1977) and Gingold & Monaghan (1977). It has been widely used in various astrophysical applications. SPH is a particle-based Lagrangian scheme: the particles' motions follow the fluid velocity. This differs from grid based methods where the fluid flow between a grid of cells is measured. An advantage of SPH is that effort is not spent solving the hydrodynamic equations in regions of space that are devoid of matter; in the case of a binary star system simulated in a grid-based code this is most of the computational volume. Another feature of SPH is that one can follow the evolution of the particles. For reviews of SPH see Benz (1990) and Monaghan (1992). Here only a few key points will be mentioned in order to show how our implementation differs from the standard technique. Our code is based upon the code of Benz (1990).

At the heart of SPH lies the kernel $W(\mathbf{r}, h)$ and the smoothing length h . These set the size and shape of a particle's sphere of influence; how much a particle affects other particles that lie at position \mathbf{r} . For example the density at \mathbf{r} is given by

$$\rho(\mathbf{r}) = \sum_{j=1}^N m_j W(|\mathbf{r} - \mathbf{r}_j|, h). \quad (1)$$

One simply takes the sum of all the particles' masses weighted by $W(|\mathbf{r} - \mathbf{r}_j|, h)$. If particle j is far from \mathbf{r} its contribution to the sum is negligible (or even zero), whilst if it is close it has a large contribution.

SPH is a Lagrangian averaging scheme so it is easy to take derivatives and hence simple to calculate the force on a particle i . For example the derivative of the density is given by

$$\langle \nabla \rho(\mathbf{r}) \rangle = \sum_{j=1}^N \frac{m_j}{\rho_j} \nabla W(|\mathbf{r} - \mathbf{r}_j|, h). \quad (2)$$

Use of a similar expression for the derivative of the pressure P and symmetrisation leads to the acceleration of a particle i ,

$$\frac{d\mathbf{v}_i}{dt} = - \sum_{j=1}^N m_j \left(\frac{P_i}{\rho_i^2} + \frac{P_j}{\rho_j^2} + \Pi_{ij} \right) \nabla W(\mathbf{r}, h) - \nabla \Phi, \quad (3)$$

where P_i is the pressure at particle i ; the first term is the symmetrized expression for the pressure gradient. The artificial viscosity Π_{ij} is introduced in SPH to improve the treatment of shocks. We use the standard formulation for this by Monaghan & Gingold (1983). We utilise a simple polytropic equation of state with $\gamma = 5/3$. Finally, $\nabla \Phi$ gives the gravitational force owing to all the other particles. For a star in stable hydrostatic equilibrium the gravitational force on a particle is balanced by the pressure gradient.

Gravity is not a local force so all particles have to be taken into account and hence a brute-force calculation scales as N^2 in the particle number. This would mean that the method would lose much of its usefulness because a large amount of computational effort would be used for the gravitational force summation. We use instead the hierarchical tree method of Benz et al. (1990) which employs a binary tree and scales as $N \log N$.

To deal better with the large range in densities that arise in simulations of these kind we employ a variable smoothing length (Benz 1990). The derivative of the smoothing length is calculated as

$$\frac{dh}{dt} = \frac{1}{3} h \nabla \cdot \mathbf{v}. \quad (4)$$

We modify the derivative thus calculated to keep the number of neighbours that each particle has between 80 and 120, subject to a maximum h of $0.1 R_\odot$.

2.2 The two phase technique: oil-on-water

A typical mass-transfer rate for a low-mass close binary is 10^{-8} to $10^{-9} M_\odot \text{ yr}^{-1}$ (Patterson 1984). This implies that, in a typical orbit of a few days to a fraction of a day, about 10^{-10} to $10^{-12} M_\odot$ is transferred. To resolve this mass flow using equal mass particles we would require at least 10^{12} of them and this is beyond what can be accomplished today. Within SPH it is possible to use a range of particle masses but if the mass range is large numerical problems arise. As an example we can consider the density calculation of Equation 1. If a particle of unit mass comes just within the range of a light particle with a mass of 10^{-4} the heavy particle dominates the density completely, even when the kernel at that point is very small. We circumvent this problem by introducing a two-phase scheme. The interior of the star is made up of heavy *water* particles while the atmosphere contains very light *oil* particles. It is these particles that take part in mass transfer. We also introduce an artificial force

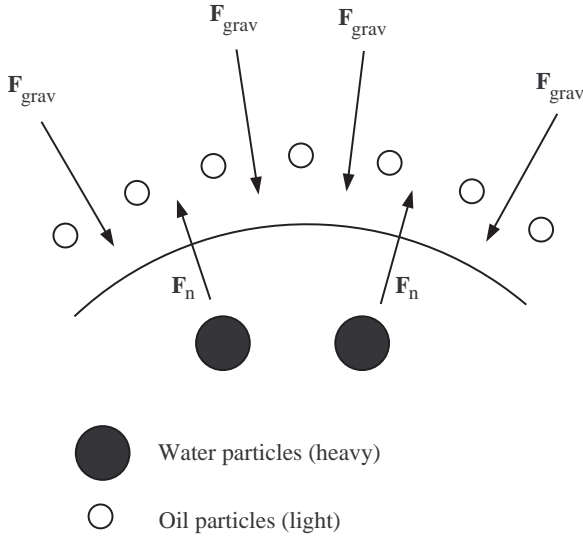


Figure 1. A cartoon figure of the force balance between the number gradient force F_n and the gravitational force F_{grav} . The number gradient of the heavy water particles introduces a force perpendicular to the surface of the star. In order for this force to be smooth a sufficient number of water particles is needed. This is accomplished, in part, by a remapping of the water particles, see Section 2.4

to keep the two different types of particles apart. This is calculated from the number gradient rather than from ∇P .

In our simulations we use 15,390 water particles to simulate a $0.6 M_{\odot}$ star so the average mass of a water particle is $3.92 \times 10^{-5} M_{\odot}$. The mass of each oil particle is $10^{-14} M_{\odot}$ so the average water particle has the same mass as 4×10^9 oil particles. We use 32,691 oil particles in our runs, so the total mass in oil particles is negligible.

Figure 1 illustrates how the oil particles are balanced on top of the water star. We have introduced an artificial force, F_n , to separate the oil layer from the water particles. This is based on the number density of the water particles and therefore is perpendicular to the edge of the water surface. This prevents the oil particles from penetrating into the stellar interior and balances their gravitational attraction to the star. It is defined according to

$$F_n = c_k \nabla n_w, \quad \nabla n_i = \sum_j \nabla_j W(|\mathbf{r} - \mathbf{r}_j|, h_{ow}) \quad (5)$$

where the sum is over the water particles j . To control the force we introduce two parameters, α and β . They are defined as

$$h_{ow} = \alpha h_w \quad (6)$$

$$c_k = \beta \frac{GM_{\odot} m_i}{R_{\odot}^2} \quad (7)$$

To calculate ∇n_i the smoothing length of the water, h_w is used rather than the usual average between the particles. A small value of α means that the oil and water particles must come closer to one another before they begin to feel the repulsive force and so the oil layer lies closer to the star. On the other hand the force must change smoothly otherwise a typical oil particle will come towards the water particles with a large velocity, bounce on the hard force barrier and get a large velocity kick away from the star. A particle's time step decreases when the rate of change of the force is large and this slows down the code. The strength of the force is controlled by β and the same arguments apply. Optimal values for the parameters

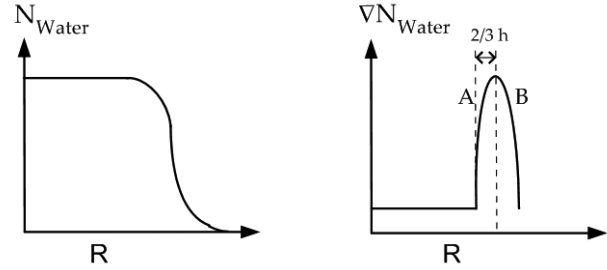


Figure 2. The left graph shows a schematic depiction of the number density of water particles computed using the SPH method. The derivative of this is shown to the right. If an oil particle comes within $\frac{2}{3}h$ of the water edge the repulsive force from the water particle density gradient declines and it can fall in towards the centre of the star.

	Force on water particle	Force on oil particle
Force from water particle	Standard	Additional force F_n
Force from oil particle	Standard	Standard

Table 1. The different force laws applied when calculating the force on a particle due to one of the others. Standard denotes the normal SPH force calculation.

have been deduced from a large number of empirical tests. For the production runs presented in this paper we use

$$\alpha = \frac{1}{2} \quad (8)$$

and

$$\beta = 40. \quad (9)$$

The force balance on the particles is then

$$\frac{d\mathbf{v}_i}{dt} = - \sum_{j=1}^N m_j \left(\frac{P_i}{\rho_i^2} + \frac{P_j}{\rho_j^2} + \Pi \right) \nabla W(\mathbf{r}, h) - \frac{\mathbf{F}_n}{m_i} - \nabla \Phi, \quad (10)$$

where the number gradient force F_n is only applied for interactions between oil and a water particles: see Table 1 for further clarification. The F_n force is similar to the normal pressure force (see Equation 3) except that the acceleration it causes has no dependence on the mass of the particles. For interactions between two oil particles or two water particles the ordinary equations are used. This is very important because the oil particles are not test particles. They obey the full SPH formalism so we can, for example, study the formation of an accretion disc around the accreting star.

2.3 The oil-water kernel

At the boundary between the oil and water particles the number density of the water particles drops quickly (see Figure 2, left panel). This gives rise to a problem with the number gradient force. Consider two oil particles located at positions A and B in the right-hand panel. If the particle at position B is perturbed slightly inwards the number density force increases and the particle is repulsed. However, if the particle at A moves inwards the number gradient decreases and the infall continues. Therefore once a particle is within $\frac{2}{3}h$ of the stellar surface it falls into the star. This can be prevented by keeping the oil particles sufficiently far away from the water edge. However this creates a separation between the oil particles and the star.

Another approach to this problem is to change the kernel for

the oil-water interaction when calculating \mathbf{F}_n . The kernel used to calculate the number gradient force does not have to be the same as that used for the rest of the calculations. Since this interaction is very different the demands on this kernel are different. The most commonly used kernel is

$$W_{\text{ML}}(r, h) = \frac{1}{\pi h^3} \begin{cases} 1 - \frac{3}{2}v^2 + \frac{3}{4}v^3 & 0 \leq v \leq 1 \\ \frac{1}{4}(2-v)^3 & 1 \leq v \leq 2 \\ 0 & \text{otherwise} \end{cases}, \quad (11)$$

where $v = r/h$ (Monaghan & Lattanzio 1985). Use of this kernel causes particles to clump together at a separation of $r = \frac{2}{3}h$. This is because the derivative of the kernel $\nabla W(r, h)$ has a minimum at this point. In our case this would imply that the oil layer is $\frac{2}{3}\alpha h$ from the edge of the water star. Because we aim to have the oil layer as close to the star as possible we investigated three other kernels,

- a kernel without a *break point* (minimum in its derivative),
- the kernel of Herant et al. (1994) and
- a kernel $W_p(r, h)$, constructed with a pair of polynomial functions, with a break point at $v_b = 0.4$.

The kernel without a break point proved unsatisfactory because as particles come close to one another the timestep falls sharply. To prevent this a large value of c_k must be used to prevent the oil particles from approaching the star. Hence the oil particles are placed far from the water surface. The other two kernels were both well-behaved but $W_p(r, h)$ seemed somewhat more robust and hence was used for our production runs presented in Section 4. It is given by

$$W_p(r, h) = \frac{1}{\pi h^3} \begin{cases} \frac{231}{142} - \frac{819}{142}v^2 + \frac{1869}{284}v^3 - \frac{315}{142}v^4 & 0 \leq v \leq 1 \\ \frac{63}{284}(2-v)^3 & 1 \leq v \leq 2 \\ 0 & \text{otherwise} \end{cases}. \quad (12)$$

To obtain this kernel, we first choose it to be the same as W_{ML} for $r > h$, subject to a normalisation factor. We construct a new fourth-order polynomial for $r < h$, subject to the constraints that

- the kernel and its first and second derivatives are continuous at $v = 1$,
- the first derivative of the kernel is zero at $v = 0$,
- the first derivative of the kernel contains only one extremum, the break point, which is a minimum, and
- the break point is located at $v_{\text{break}} < \frac{2}{3}$ (we choose $v_{\text{break}} = 0.4$).

These conditions specify the kernel W_p up to the standard normalisation factor.

2.4 Remapping of the water particles

It is advantageous to have as many water particles as possible in the outer parts of the star and hence close to the interface of the oil and water particles. This can be accomplished by remapping the water particles to increase the number density at the edge of the star. The star is initially built up using a close-packed lattice with the water particles placed equidistantly. Particle masses are assigned to obtain the correct density profile, following the YREC-models of Guenther et al. (1992). To increase the concentration of water particles at the surface we remap their positions according to a power law of index $\gamma = 0.9$. Each particle i is updated according to

$$r_{i,\text{remap}} = c_{\text{norm}} r_i^\gamma \quad (13)$$

where c_{norm} is a normalisation factor to keep the stellar radius constant. This increases the number density at the outer edge by a factor of about 1.25 with respect to the centre. The larger number of water particles at the edge makes the surface smoother; this allows us to place the oil layer closer to the surface.

2.5 Production of the single-star models

To build a star the water particles are first set up using the procedure described above. The resulting model is then relaxed for approximately $100 \tau_{\text{relax}}$, where τ_{relax} is the dynamical timescale given by

$$\tau_{\text{relax}} = \sqrt{\frac{R_\odot^3}{GM_\odot}} \quad (14)$$

Then the oil layers are added on top of the relaxed water star. We have tried different numbers of oil particles: one and three layers of oil require 9,983 and 32,691 oil particles respectively. These are added according to a close-packed lattice with a spacing equal to the internal smoothing length, $h = 0.025 R_\odot$. The oil particles each have a mass of $10^{-14} M_\odot$. The model is relaxed until the particles have settled into a stable configuration; this typically takes about $50 \tau_{\text{relax}}$.

The two stars with one and three layers of oil are shown in Figure 3. In the model that originally had a single layer the oil particles are evenly spread around the star but there is no depth in the oil layer. The other has visible structure. The oil particles all have the same mass so density is well-mapped by the number density of the oil particles. There are more oil particles close to the water-oil boundary so the atmosphere is densest here. The simulations presented here all utilise 32,691 oil particles as in the three-layer model. The remapping of the water particles is also visible in the density contrast between the centre and surface of the water particle star.

3 CIRCULAR BINARIES

In order to test the reliability of the oil-on-water model we used the code to model circular binary systems. Because the potential field is circular, co-rotating binaries is well described by the Roche formalism there is a large body of work that describes them and hence useful comparisons may be made. Two questions can be posed. First, can we make a binary system that reproduces observed properties correctly? Second, how much does the unphysically large size of the atmosphere in our models affect the results that we obtain? We answer these two questions by making models of a cataclysmic variable system in the manner described below.

3.1 The Roche potential

In a circular binary where one star is filling its Roche lobe, the mass flow is continuous and steady, and a number of simplifications can be made. By assuming that the stars are centrally condensed for the purposes of calculating the potential and that they are corotating with the orbit we obtain the Roche potential (Pringle & Wade 1985). In a corotating frame centred on star 1, with the line connecting the two stellar centres along the x axis, the potential takes the form

$$\Phi_R(x, y, z) = -\frac{GM_1}{\sqrt{x^2 + y^2 + z^2}} - \frac{GM_2}{\sqrt{(x-a)^2 + y^2 + z^2}}$$

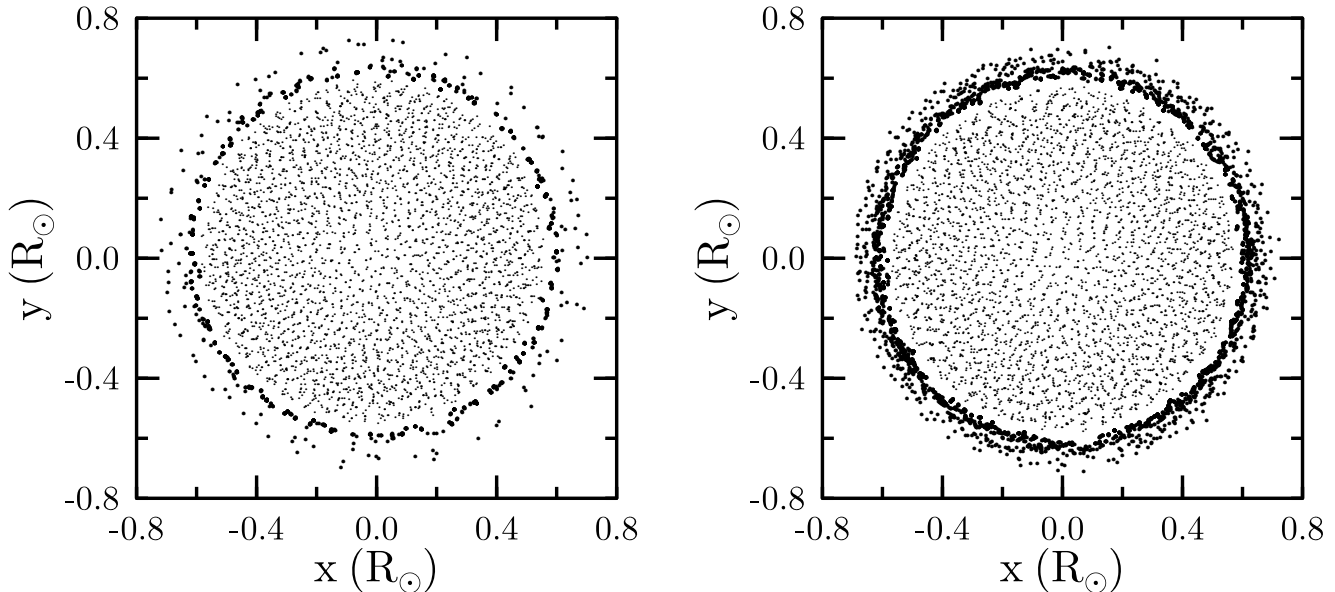


Figure 3. Two examples of a relaxed composite star. The particles plotted are those within h of the xy plane. The small dots are water particles and the large dots oil particles. In both models there are 15,390 water particles. In the left-hand model there are 9,983 oil particles: in the right-hand 32,691. In the right-hand figure a clear density structure can be seen in the oil particles.

$$-\frac{1}{2}\Omega_C^2 [(x - \mu a)^2 + y^2], \quad (15)$$

where a is the separation, Ω_C the angular velocity and the reduced mass $\mu = M_2/(M_1 + M_2)$. The last term in this expression is due to the centrifugal force. The stationary point between the two stars is the inner Lagrangian or L1 point, and the surface around each star that passes through this point is its Roche lobe. The radius of a spherical star with the same volume as its Roche lobe is called the Roche-lobe radius R_L and is fitted within a few per cent by

$$\frac{R_L}{a} = \frac{0.49q^{2/3}}{0.6q^{2/3} + \ln(1 + q^{1/3})}, \quad (16)$$

(Eggleton 1983), where $q = M_2/M_1$ is the mass ratio. If one of the stars fills its Roche lobe mass flows through L1 to the other star. Ritter (1988) showed that the amount of mass transferred in a binary system depends on the pressure scale height H_p of the donor star's atmosphere and the difference between the donor star's radius R and R_L , according to

$$\dot{M} = \dot{M}_0 e^{-(R_L - R)/H_p}, \quad (17)$$

where \dot{M}_0 is the mass-transfer rate of a binary that just fills its Roche lobe. For a low-mass main-sequence star $\dot{M}_0 \approx 10^{-8} M_\odot \text{ yr}^{-1}$ and $H_p \approx 10^{-4} R_\odot$.

3.2 Production of circular binary models

The transition from the spherical potential produced by the self-gravity of a single star and the Roche potential owing to an orbiting binary system disrupts the structure of our relaxed star unless care is taken. For this reason it is necessary to relax a binary system once the star has been placed in its orbit before allowing mass transfer to proceed. To do this we first add a point mass to the star to represent a compact companion. In all these runs we have used a star with mass $0.6 M_\odot$ and a $1 M_\odot$ point mass. Initially we place the star and point mass in a frame rotating about the centre of mass with

a damping force in place to allow the star to adjust to the gravitational field of the point mass. The star is taken to be co-rotating: it is stationary in the rotating frame other than for oscillations during relaxation. Once the star has relaxed the model and point mass are transformed back into an inertial frame. The star and the point mass are both given the correct velocities to place them on the desired orbit. Relaxation takes approximately $10 \tau_{\text{relax}}$.

For an eccentric mass-transfer binary the relaxation takes place in a circular orbit at the apocentre separation where no mass transfer takes place. In contrast for a circular orbit the separation of the stellar centre and point mass is constant and hence there is no point in the orbit at which the relaxation can take place without mass transfer occurring. To avoid this problem we relax the star in a circular orbit that is slightly wider than the widest orbit in which appreciable mass transfer takes place. After relaxation the separation of the orbit is reduced by 0.5% each dynamical timescale, changing the positions and velocities of the particles. This provides a series of circular models at different separations that can be evolved further to model a series of binaries.

At low mass-transfer rates we encounter numerical problems. Because the rate of flow of particles into the accretor's Roche lobe is small there are only a few particles present, which causes the pressure forces to vary very rapidly. These particles gain large velocities and are ejected from the Roche lobe. To counter this problem we turn off sph forces for oil particles with fewer than 50 neighbours: that is, such particles move ballistically.

3.3 Results

All the circular binaries consisted of a $0.6 M_\odot$ star, modelled using the two-phase oil-on-water technique and a $1 M_\odot$ point mass. Such binaries are believed to be relatively high-mass cataclysmic variable (CV) systems. In these hydrogen-rich material accretes on to a white dwarf and burns explosively at the surface. Ongoing mass transfer is thought to be driven by angular momentum loss owing to either a magnetic wind or gravitational radiation. Observations

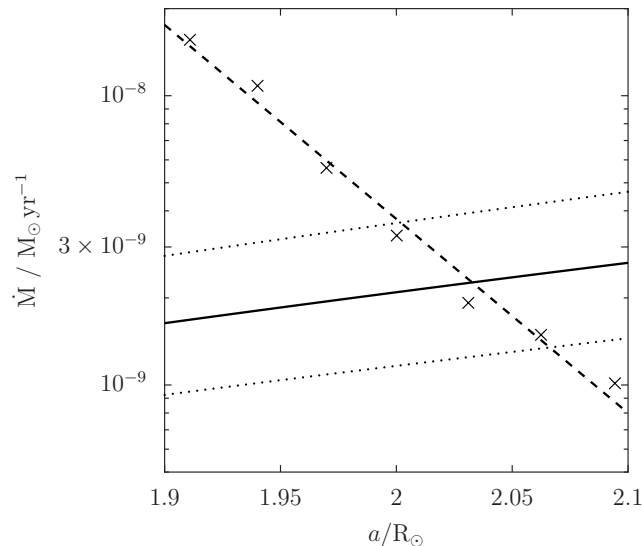


Figure 4. The mass-transfer rate in our circular binary models. The crosses show the rate at which mass is accreted in the circular systems and the dashed line is a straight-line fit to these points. The solid line is the observed accretion rate for CVs from Equation 17 of Patterson (1984), and the dotted lines its 1-sigma error interval.

of many such systems have been made and their accretion rates can be measured from their luminosities. We ran models at a range of separations, which yielded a corresponding range of mass-transfer rates. We measure the rate by fitting the number of particles in the Roche lobe of the accretor as a linear function of time, using a standard least-squares fitting algorithm. The accretion rate for a given binary was roughly constant until a substantial fraction of the envelope had been transferred. The accretion rates we obtain are shown in Figure 4, along with an observational measurement of the CV accretion rate from Patterson (1984).

Mass transfer from a CV is driven by a loss of angular momentum from the system and the mass-transfer rate is seen to be a function of the binary period. At the points where the observed accretion rates and the accretion rates obtained from our code are equal we can take the separation to be that predicted for the CV we are modelling. We find this equilibrium separation to be $a = 2.03^{+0.04}_{-0.03} R_{\odot}$. Applying Equation 16 with $q = 0.6$ gives a Roche lobe radius $R_L = 0.68^{+0.015}_{-0.01} R_{\odot}$. The mean volume of the star, as defined by the volume occupied by the water particles, was estimated by finding its extreme points along the three natural axes of the system and calculating the volume of an ellipsoid with those axis lengths. The radius of the sphere with the same volume, in analogy to the definition of the Roche lobe radius, is $0.57 R_{\odot}$. If we assume that the real edge of the star coincides with the outer surface of the water particles this gives an error in the effective radius of the stellar model owing to the extended atmosphere of 15 to 18%.

The mass-transfer rate in our models varies in an approximately exponential fashion with separation. Hence the model shows the qualitative behaviour predicted by Ritter (1988), which suggests that the atmosphere is sufficiently resolved. By rearranging Equation 17 and substituting for the Roche lobe radius from Equation 16 with $q = 0.6$ we obtain

$$\log\left(\frac{\dot{M}}{M_0}\right) = \frac{R}{H_p} - 0.3356 \frac{a}{H_p}. \quad (18)$$

Equating the final term to the variation in accretion rate from Fig-

Table 2. A table of the runs with different semi-major axes a and eccentricities e . In all cases the mass ratio $q = 0.6$. Column 4 indicates whether no mass transfer (N), mass transfer (Y) or massive mass transfer (M) was observed. For the mass-transfer case the number of particles escaping the donor per orbit is given in Column 5.

a/R_{\odot}	e	$r_{\text{peri}}/R_{\odot}$	Mass transfer	Oil particles lost from donor per orbit
2.5	0.0	2.500	N	-
2.5	0.15	2.125	Y	30
2.5	0.20	2.000	Y	200
2.5	0.25	1.875	Y	500
3.0	0.0	3.000	N	-
3.0	0.15	2.550	N	-
3.0	0.30	2.100	Y	20
3.0	0.35	1.950	Y	200
3.0	0.375	1.875	M	-
3.0	0.40	1.800	M	-
4.0	0.40	2.400	N	-
4.0	0.45	2.200	N	-
4.0	0.50	2.000	Y	40
4.0	0.525	1.900	Y	250
4.0	0.55	1.800	M	-
5.0	0.50	2.500	N	-
5.0	0.60	2.000	Y	10
5.0	0.625	1.875	M	-
5.0	0.65	1.750	M	-
6.0	0.65	2.100	N	-
6.0	0.675	1.950	Y	50
6.0	0.6875	1.875	M	-
6.0	0.70	1.800	M	-
7.0	0.70	2.100	N	-
7.0	0.75	1.750	M	-
8.0	0.75	2.000	Y	60

ure 4 gives an effective pressure scale height of $0.022 R_{\odot}$, unsurprisingly very similar to the smoothing length h . The pressure scale height of a low-mass main-sequence star is about $10^{-4} R_{\odot}$, roughly two orders of magnitude smaller than in our models. This means that the onset of mass transfer in our models will be much gentler than that seen in real systems.

4 ECCENTRIC BINARIES

To simulate eccentric binaries we carried out a grid of runs with different a and e . In each case the donor was a main-sequence star of $M = 0.6 M_{\odot}$ and the accreting companion was a white dwarf with $M = 1 M_{\odot}$. To relax the star the point mass was initially placed at a distance a_{apo} from the star in a circular orbit as explained above. When the system had relaxed sufficiently we released it from co-rotation and introduced eccentricity in such a way that it was relaxed at apocentre: the spin of the star was set to coincide with the angular velocity of the system there. Therefore the star initially co-rotates at apastron. The spin rate is not found to change significantly during a complete run. Figure 5 is an example of a system with $a = 2.5 R_{\odot}$ and $e = 0.2$ which undergoes mass transfer only at

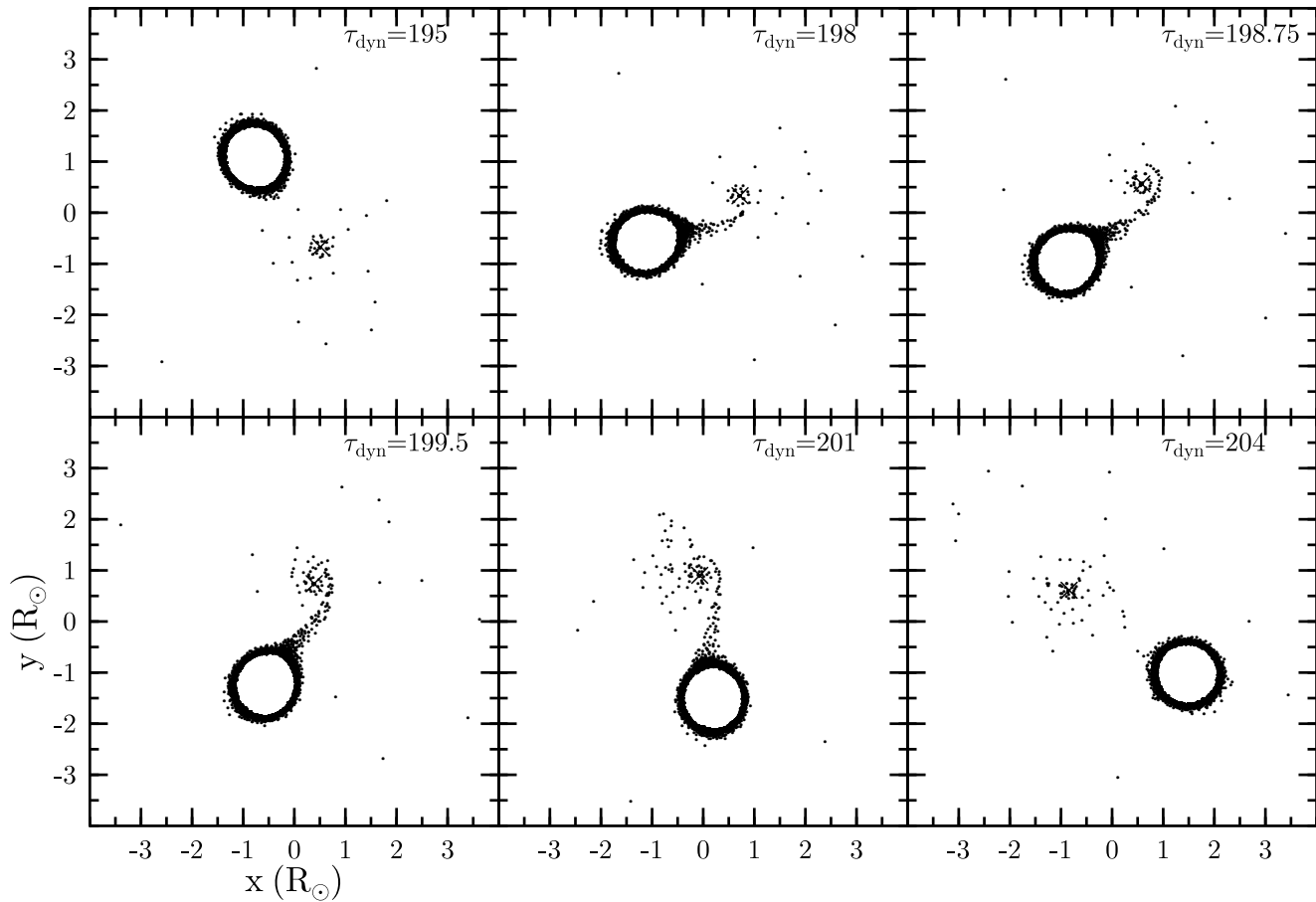


Figure 5. An example of mass transfer in an eccentric binary with $a = 2.5 R_{\odot}$ and $e = 0.2$. Here for clarity only oil particles within h of the xy -plane are plotted. The position of the point-mass companion is marked with a cross. The mass of the star is $0.6 M_{\odot}$ and that of the point mass $M = 1.0 M_{\odot}$, as in all the simulations in this paper. In this binary mass is transferred only near periastron, which occurs when the star is to the left of the point-mass along the x -axis. This image sequence starts just before periastron passage and, as the star approaches periastron the mass transfer begins; however there is a noticeable lag. The mass transfer actually begins just after the closest approach and continues for almost $1/4$ of the orbit.

periastron, so the mass transfer turns on and off in each orbit. One such mass-transfer event is shown.

Table 2 enumerates parameters for the grid of runs completed, stating whether mass transfer takes place and, if so, the number of oil particles escaping the donor star per orbit. More eccentric systems have a narrower range of a in which stable mass transfer takes place. This is expected because the periastron separation is given by $a_p = a(1 - e)$, so a small change in e leads to a large change in the periastron separation.

An example of the mass transfer in one of our runs is given in Figure 6. The periodic behaviour of the mass transfer is apparent. On each orbit mass begins to flow from the donor at pericentre. The number of oil particles lost from the donor at each periastron passage is roughly constant after the first few orbits. This indicates that the mass transfer is stable. One periastron passage of this system is also pictured in Figure 5.

Our models are plotted in the (a, e) -space in Figure 7. Open circles denote systems without mass transfer, filled circles stable mass transfer and crosses denote that there is a massive overflow of particles with water particles being transferred. The prediction of Equation 16 for an instantaneous Roche lobe at pericentre is also plotted. Such an approach assumes that the timescale of the mass transfer is sufficiently fast to be able to adjust to the instantaneous distance and rotational velocity. The typical orbital passage

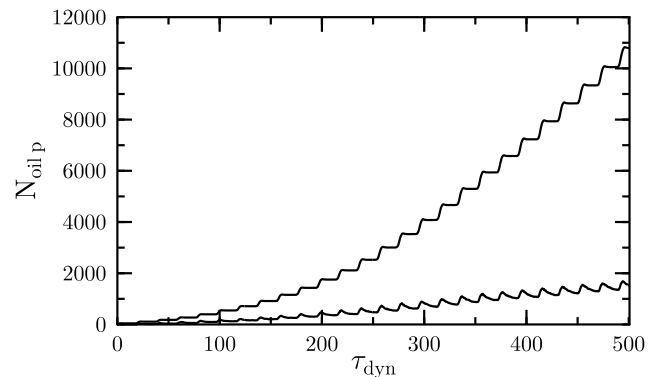


Figure 6. The cumulative number of oil particles released from the donor against time in the case of an eccentric system ($a = 2.5 R_{\odot}$, $e = 0.2$). After the first initialisation, where a damping force is active, there is a stable flow of particles at periastron and this gives rise to the stepped function. The lower curve shows the number of particles captured by the companion. Most of the particles transferred are not captured but escape through L2. As discussed in section 3.1 the potential at L2 is almost the same height as the inner Lagrangian point L1 for $e = 0.25$

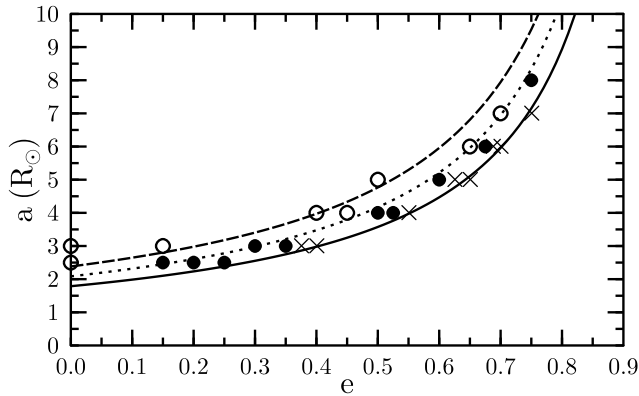


Figure 7. Results from runs at different a and e . Open circles denote binaries where no mass transfer was seen, filled circles are runs with stable mass transfer, and crosses mark models where a massive overflow of particles was observed and water particles began to transfer. The curves show the separations derived for the onset of mass transfer under the assumption that the star exactly fills its Roche lobe at periastron. The three curves are for stellar radii of 0.6, 0.7 and 0.8 R_{\odot} , with 0.8 R_{\odot} being the topmost curve.

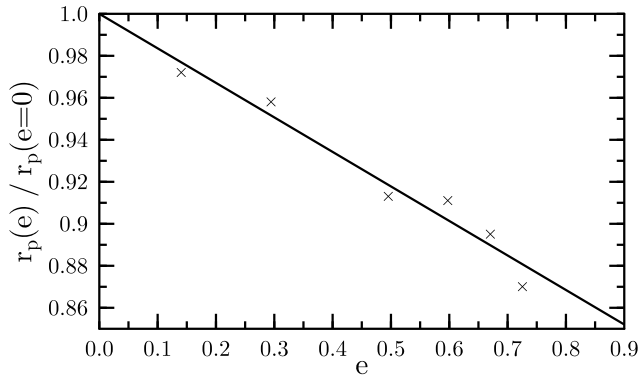


Figure 8. The ratio $r_p(e)/r_p(e=0)$ as a function of the eccentricity. The separation required for onset of mass transfer for different eccentricities is $r_p(e)$. The line is a linear fit to the points, given by $f(e) = 1 - 0.16e$.

shown in Figure 5 shows that this is not the case. The mass transfer does not begin until just after periastron passage and continues for almost 1/4 of an orbit thereafter. This is due to the time taken for the material to respond to the changing potential as the star goes round the periastron passage and the time taken for matter to flow from the donor to the companion. The instantaneous Roche lobe construction also assumes corotation, which only can be true at one point in the orbit.

In order to quantify the effect of the eccentricity we express the periastron distance required for onset of mass transfer, $r_p(e)$, as

$$r_p(e) = r_p(e=0) \times f(e), \quad (19)$$

where $r_p(e=0)$ is the separation required for the circular case and $f(e)$ is a correction function to be determined. If the instantaneous Roche lobe formalism was applicable, i.e. the onset of mass transfer was determined by the Roche lobe at periastron, we would obtain $f(e) = 1$. Based on our runs in Table 2 we have estimated the eccentricity for which the mass transfer begins for a given semi-major axis a . The results are plotted in Figure 8. We have extrapolated the data to $e = 0$ to obtain an estimate of the periastron distance at which mass transfer starts in the circular case as $r_p(e=0) = 2.212 R_{\odot}$. The required distance for onset of mass

transfer between the stars can be seen to decrease with increasing eccentricity. The line is a linear fit to the points which yields $f(e) = 1 - 0.16e$. Equation 19 expressed in terms of the semi major axis a gives

$$a_{mt}(e) = a_{mt}(e=0) \times \frac{1 - 0.16e}{1 - e}, \quad (20)$$

where $a_{mt}(e)$ is the required semi major axis for mass transfer and $a_{mt}(e=0)$ can be obtained from Equation 16. Note however that in our simulations all runs are corotating at apastron and $q = 0.6$, so the formula given above is only tested for this case.

5 CONCLUSIONS AND FUTURE PROSPECTS

The simulation of mass transfer in eccentric binaries is non-trivial because the mass transferred in each orbit is a tiny fraction of the total mass. In this article we have presented a technique that treats this problem by introducing a two-phase SPH formalism. Very light particles make up the outer part of the donor star, while the inner part is formed from heavier particles. Thanks to this oil-on-water model we have been able to simulate mass transfer in eccentric binaries. The simulations presented here cover a large range of semi-major axes and eccentricities at a mass ratio of 0.6.

We have found that the onset of mass transfer in our simulations does not follow the prescription of the circular case. We have measured the eccentricity required for mass transfer given a semi-major axis a . Using this we show that the minimum distance between the stars that leads to mass transfer decreases linearly with eccentricity.

The oil-on-water model could be used to simulate other interesting astrophysical processes. One example is the onset of common envelope evolution. A close binary system undergoes a common envelope (CE) phase if the secondary star is unable to accrete all the mass transferred by the donor (Paczynski 1976; Rasio & Livio 1996). The core of the evolved star and the secondary orbit one another in a cloud of gas, which is eventually expelled. This transports angular momentum away from the system and the period of the system decreases. The oil-on-water technique can follow the angular momentum transferred at the onset of the common envelope phase accurately, making it an useful tool for such an investigation.

ACKNOWLEDGEMENTS

The authors would like to thank the referee, Phil Armitage, for his constructive comments on the manuscript. RPC would like to thank the Swedish Institute for a Guest Scholarship. MBD is a Royal Swedish Academy Research Fellow supported by a grant from the Knut and Alice Wallenberg Foundation. CAT thanks Churchill College for a Fellowship.

REFERENCES

- Benz W., 1990, in Numerical Modelling of Nonlinear Stellar Pulsations Problems and Prospects Smooth Particle Hydrodynamics - a Review. p. 269
- Benz W., Cameron A. G. W., Press W. H., Bowers R. L., 1990, ApJ, 348, 647
- Binney J., Tremaine S., 1987, Galactic dynamics. Princeton, NJ, Princeton University Press, 1987, 747 p.

- Boyle C. B., Walker I. W., 1986, *MNRAS*, 222, 559
- Brandt N., Podsiadlowski P., 1995, *MNRAS*, 274, 461
- Brown J. C., Boyle C. B., 1984, *A&A*, 141, 369
- Charles P. A., Booth L., Densham R. H., Bath G. T., Howarth I. D., Willis A. J., Skinner G. K., Thorstensen J. R., Olszewski E., 1983, *MNRAS*, 202, 657
- Clarkson W. I., Charles P. A., Onyett N., 2004, *MNRAS*, 348, 458
- Davies M. B., Benz W., 1995, *MNRAS*, 276, 876
- Davies M. B., Benz W., Hills J. G., 1994, *ApJ*, 424, 870
- Eggleton P. P., 1983, *ApJ*, 268, 368
- Gingold R. A., Monaghan J. J., 1977, *MNRAS*, 181, 375
- Guenther D. B., Demarque P., Kim Y.-C., Pinsonneault M. H., 1992, *ApJ*, 387, 372
- Guseinov O. H., Saygac A. T., Allahkverdiev A., Caliskan H., Ozdemir S., Yerli S. K., Anday A., 2000, Technical report, X-Ray Binaries Catalogue
- Haynes R. F., Lerche I., Wright A. E., 1980, *A&A*, 81, 83
- Herant M., Benz W., Hix W. R., Fryer C. L., Colgate S. A., 1994, *ApJ*, 435, 339
- Ivanova N., 2006, *ApJ*, 636, 979
- Johnston H. M., Fender R., Wu K., 1999, *MNRAS*, 308, 415
- Kretschmar P., Wilms J., Staubert R., Kreykenbohm I., Heindl W. A., 2004, in Schoenfelder V., Lichti G., Winkler C., eds, *ESA SP-552: 5th INTEGRAL Workshop on the INTEGRAL Universe XMM-Newton Observations of the Be/X-Ray Transient A0538-66 in Quiescence*. pp 329–+
- Lucy L. B., 1977, *ApJ*, 82, 1013
- Monaghan J., Gingold R., 1983, *J. Comp. Phys.*, 52, 374
- Monaghan J. J., 1992, *ARA&A*, 30, 543
- Monaghan J. J., Lattanzio J. C., 1985, *A&A*, 149, 135
- Murdin P., Jauncey D. L., Lerche I., Nicolson G. D., Kaluzinski L. J., Holt S. S., Haynes R. F., 1980, *A&A*, 87, 292
- Paczyński B., 1971, *ARA&A*, 9, 183
- Paczynski B., 1976, in Eggleton P., Mitton S., Whelan J., eds, *IAU Symp. 73: Structure and Evolution of Close Binary Systems Common Envelope Binaries*. pp 75–+
- Patterson J., 1984, *ApJS*, 54, 443
- Pringle J. E., Wade R. A., 1985, *Interacting binary stars*. Cambridge University Press
- Rasio F. A., Livio M., 1996, *ApJ*, 471, 366
- Regös E., Bailey V. C., Mardling R., 2005, *MNRAS*, 358, 544
- Renvoizé V., Baraffe I., Kolb U., Ritter H., 2002, *A&A*, 389, 485
- Ritter H., 1988, *A&A*, 202, 93
- Ritter H., Kolb U., 2006, *VizieR Online Data Catalog*, 1, 2018
- Tauris T. M., Fender R. P., van den Heuvel E. P. J., Johnston H. M., Wu K., 1999, *MNRAS*, 310, 1165
- Verbunt F., 1993, *ARA&A*, 31, 93